Lateral ordering, strain, and morphology evolution of InGaAs/GaAs(001) quantum dots due to high temperature postgrowth annealing

M. Riotte,[1,a] E. Fohtung,[1] D. Grigoriev,[2] A. A. Minkevich,[1] T. Slobodskyy,[1] M. Schmidbauer,[3] T. H. Metzger,[4] D. Z. Hu,[5] D. M. Schaadt,[5] and T. Baumbach[1,2]
[1]*ANKA/Institute for Synchrotron radiation, Karlsruhe Institute of Technology, 76344 Eggenstein-Leopoldshafen, Germany*
[2]*Laboratory for application of synchrotron radiation, Karlsruhe Institute of Technology, Germany*
[3]*Leibniz-Institut für Kristallzüchtung, Max-Born-Straße 2, D-12489 Berlin, Germany*
[4]*European Synchrotron Radiation Facility, B.P. 220, F-38043 Grenoble Cedex, France*
[5]*Institute for Applied Physics/DFG-Center for Functional Nanostructures, Wolfgang-Gaede-Str.1a 76131 Karlsruhe, Germany*

(Received 5 November 2009; accepted 4 January 2010; published online 23 February 2010)

The effect of postgrowth annealing on shape and ordering of a single layer of InGaAs/GaAs(001) quantum dots is investigated by three dimensional grazing incidence small angle x-ray scattering. A transition from disordered dots to two-dimensional lateral ordering is found. This transition is accompanying a quantum dot shape transformation. Grazing incidence diffraction measurements relate the observed ordering type to strain driven self organization. The role of different growth conditions leading to lateral correlation is discussed by comparing the results to recent experimental achievements in the field. © *2010 American Institute of Physics*. [doi:10.1063/1.3299262]

Semiconductor quantum dots (QDs) are intensively investigated because of their unique optoelectronic properties leading to a wide range of applications such as optimized light emitting diode structures,[1] efficient solar cells,[2,3] tailoring of laser emission,[4] or quantum computing and data storage devices.[5] Many devices require QDs with well defined size, shape, and controllable spatial ordering. Strain-driven self assembly has been shown to be suitable for this purpose.[6,7]

Self organization phenomena of positional correlation of QDs are usually studied in *multilayers* where strain driven ordering occurs progressively during the multilayer growth.

In case of InGaAs QDs on GaAs(001) two different ordering types were found so far. The first type is a one-dimensional (1D) twofold symmetric arrangement in chains elongated along $[1\bar{1}0]$.[6] The second type is a two-dimensional (2D) fourfold symmetric arrangement along the [100] and [010] axis.[8] In case of InGaAs QDs on (311B) substrates two analog types of correlation have been observed.[9,10] For QD multilayer structures several publications report a transition from one to the other correlation type. This transition in the multilayer parameter space could be achieved by changing the substrate surface orientation,[11] the spacer layer thickness,[9] and the number of layers.[8]

The effect of self ordering is most commonly explained by interplay of several factors such as crystallographic orientation, structure, and temperature of the substrate, vertical and lateral material transfer (growth rate, in-plane mobility of ad-atoms), and several multilayer parameters.

The key mechanism of self-organization is usually attributed to the anisotropic elastic forces between the dots. The strain field induced by the QDs inside the surrounding host material was highlighted several times as driving force for positional correlation.[7,12,13] Ordering helps to minimize the strain mediated elastic interaction energy between neighboring islands.

Clearly the multilayer sequences supports the ordering. However, already for a *single* layer of InGaAs QDs on GaAs(001) ordering phenomena[8] have been reported. The conditions fostering the occurrence of ordering already in the first layer therefore gain interest.

The present work studies shape and ordering for the case of single layer InGaAs QDs on GaAs(001). We report the evolution of shape and ordering during postgrowth annealing. The study combines atomic force microscopy and strain and shape sensitive x-ray methods to gain insight into the mechanism of ordering.

Samples were prepared in a Riber 21 compact molecular beam epitaxy system. Epiready GaAs(001) substrates were degassed at 150 °C for 1 h in a load lock chamber. Oxide desorption was carried out by keeping substrates at 600 °C for 20 min under constant As_4 flux. The 2×4 surface reconstruction was clearly observed in the reflection high-energy electron diffraction pattern. A 250 nm thick GaAs buffer layer was deposited at 570 °C followed by the deposition of 2.1 monolayer (ML) InAs at 500 °C. The growth rates of GaAs and InAs are 0.44 and 0.068 ML/s, respectively. We compare two samples: One sample stayed unannealed since it was rapidly cooled to room temperature. The other sample was kept at growth temperature for 5 min under constant As_4 flux and then rapidly cooled. After removal from the ultra-high vacuum (UHV) system the samples were covered with protective photo resist.

X-ray scattering measurements were performed with synchrotron radiation at the ESRF beamlines ID10B and ID01, and the ANKA beamline SCD. Shortly before starting measurements the photoresist was removed and the samples were placed inside a protective environment. Grazing incidence small angle scattering (GISAXS) was carried out at a wavelength of $\lambda=1.53$ Å making use of a position sensitive line detector in combination with a Si(111) analyzer. Grazing incidence diffraction (GID) was performed at $\lambda=1.5028$ Å

[a]Electronic mail: markus.riotte@iss.fzk.de.

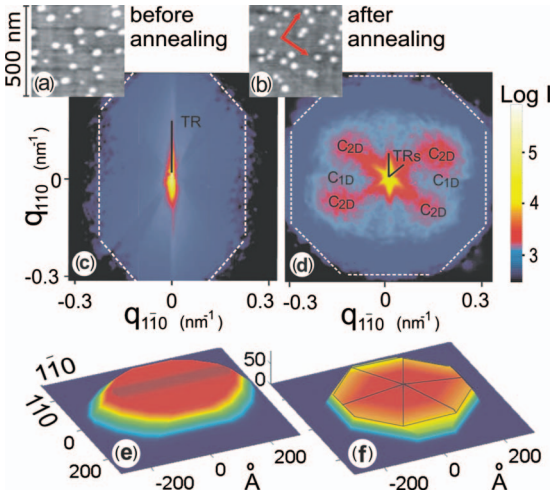

FIG. 1. (Color) Detail of the atomic force micrographs (500×500 nm^2) showing the QDs (a) before and (b) after annealing. The red arrows in (b) indicate the direction of QD positional correlation. Two color maps (c) and (d) display the measured in-plane GISAXS data of the corresponding samples in (a) and (b). (α_i=0.7 and 0.8°). The 3D models propose the shape of the QDs (e) before and (f) after annealing.

based on a microfocused incident beam ($1.2\ \mu m\times2.5\ \mu m$) and recording the diffraction pattern by a 2D charge coupled device detector. This arrangement ensured quite fast data recording with sufficient resolution.

The atomic force microscopy (AFM) analysis reveals that the mean density of the dots decreased considerably from 92 to 56 μm^{-2} after annealing, while the mean size decreased slightly from 56 to 48 nm. The average height also decreased from 7.5 to 5 nm. This confirms findings in literature where coarsening of dots has been observed at the beginning of annealing treatment while after critical annealing time a decrease in height and radius occurs due to enforced In desorption.[14,15] Within the accessible scanned area of a $5\times5\ \mu m^2$ AFM image, the Fourier transform (FT) analysis did not display any clear positional correlation neither before nor after annealing.

X-ray scattering experiments have an increased sensitivity to positional correlations as the large footprint of the x-ray beam on the sample during the GISAXS measurements enables good statistical averaging. Correlation of positions of self-assembled QDs give rise to corresponding maxima of the scattered intensity distribution in reciprocal space.[16]

Figure 1 shows two color maps (c) and (d) of the measured in-plane GISAXS intensity distribution in reciprocal space. Clear identification of relevant scattering contributions was done by 3D analysis. The visualization is afterwards possible by projecting the measured 3D intensity distribution onto the $q_{110}/q_{1\bar{1}0}$ plane along the q_{001} interval from 0.4 to 0.75 nm^{-1}. Thereby enhanced diffuse scattering at the Yoneda wings ($\alpha_f=\alpha_c$) is included and the coherent specular reflection peak ($\alpha_f=\alpha_i$) is excluded (where α_i, α_f, and α_c are the incident and exit angles, and the critical angles of total external reflection).

Three main features can be observed in the GISAXS pattern. Side facets of QDs generate truncation rods (TR). The yellow shafts in the center of the maps are projections of these TRs onto the $q_{110}/q_{1\bar{1}0}$ plane. The clouds of diffuse scattering (blue areas indicated by the dashed lines) contain the squared FT of the QD shape. From the symmetry of the clouds we can establish the symmetry of the QD shape in real space. Positional correlation maxima C_{2D} are visible on the image (d) of Fig. 1, related to the covariance functions of the scattered wave amplitudes.

In image (c) TR projections of two side facets are clearly visible while six TRs of side facets appear after annealing (d). The in-plane directions of the TRs in reciprocal space directly indicate the crystallographic orientation of the corresponding QD side facets. The full 3D analysis resulted in (119), ($\bar{1}\bar{1}9$) faceted dots before (e) and (117), ($\bar{1}17$), (107), ($\bar{1}07$), (017), ($0\bar{1}7$) faceted QDs after annealing (d). Appearance of {117} facets after postgrowth annealing at 500 °C was reported recently.[15] The substrate TR contributes only to the central intensity spots as it is oriented perpendicular to the plane of projection.

The blue cloud in (c) is elongated if compared to (d). This is a fingerprint of the elongated base along $[1\bar{1}0]$ in case of the nonannealed QDs. Elongated shaped dots are typical for this material system. The reason for this shape asymmetry is the anisotropy of the adatom surface diffusion.[8] Due to surface reconstruction[8] the Indium diffusion coefficient $D_{1\bar{1}0}$ is much larger than D_{110}.[17] In case of the annealed sample (panel d) the blue cloud in the GISAXS pattern has the shape of a rounded octagon. No essential difference between the extension along the $[1\bar{1}0]$ and the [110] direction exists any more. From this we conclude that the annealing procedure gave time to compensate the limited diffusion length in the [011] direction and therefore the base shape of the dots became more highly symmetrical.

The nonannealed sample (c) does not show any positional correlation while four correlation peaks C_{2D} positioned along [010] and [100] are clearly identified in case of the annealed sample (d). The distance between opposite peaks is 0.34 nm^{-1} which corresponds to 37 nm in real space and reveals a close neighboring as it is also confirmed by AFM. From the peak width $\delta_{q_{\mathrm{rad}}}=0.05$ nm^{-1} we can evaluate a short range ordering correlation length of about $\Lambda_{\mathrm{rad}}=2\pi/\delta_{q_{010}}=125$ nm which is smaller than the Indium adatom diffusion length of $1-2\ \mu m$ according to Ref. 18. It is difficult to provide exact numbers for the diffusion length in our case since there is an interplay between QD strain-fields[19] and surface reconstruction. Even if all positions of the correlation peaks are slightly compressed toward C_{1D} correlation the findings give evidence for dominant 2D dot-dot ordering extending over three to four QDs.

The strain field around dots is determined by both the elastic properties of the host crystal and by the shape of the dot. The elastic property of bulk GaAs has fourfold symmetry in the (001) plane. In Ref. 8 it was shown that in case of elongated dots the shape contribution is different along $[1\bar{1}0]$ and along [110]. Therefore the symmetry of the strain field around the dots is reduced from fourfold to twofold explaining the finding of twofold symmetric correlation for such structures.

Our measurements, however, give clear evidence for the formation of a dominant fourfold symmetric correlation type after annealing, simultaneously we observe dots with rounded octagonal bases. Thus the shape contribution to strain is nearly identical in both, the [110] and $[1\bar{1}0]$ direction, and the symmetry of the strain field around the dots is

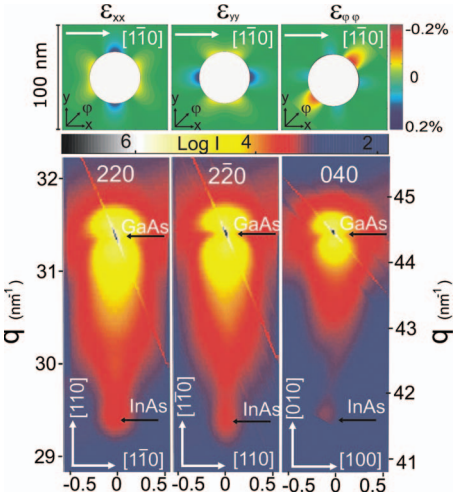

FIG. 2. (Color) Upper part: CEM of the strain around a Quantum Dot. Three components of the strain tensor ϵ_{xx}, ϵ_{yy}, and $\epsilon_{\varphi\varphi}$ are plotted. The coordinates x, y, φ correspond to the crystallographic directions [1$\bar{1}$0], [110], and [010]. Lower part: GID measurements around the [2$\bar{2}$0], [220], and [040] reflection (α_i=0.35°).

close to fourfold one as expected from the elastic properties of InAs and GaAs for (001) substrate.

The results of analytical strain simulation in the upper part of Fig. 2 illustrate this symmetry. Here the strain field around a dot with a round base has been calculated based on a continuum elasticity model (CEM).[20] It can be seen that for elastically equivalent [110] and[1–10] directions the corresponding strain components ϵ_{xx} and ϵ_{yy} are complementary, corresponding to a fourfold symmetric lattice displacement field.

The GID measurements in Fig. 2, lower part, confirm this behavior, since we measured nearly identical intensity distributions in the reciprocal space maps around the [220] and [2$\bar{2}$0] reflections. Comparing the CEM calculations of the strain component $\epsilon_{\varphi\varphi}$ (oriented along [010]) to the previous we find strong differences. And, in accordance with this, the GID intensity map around the [040] reflection differs strongly from the other maps (all maps are normalized by structure factors). The smooth peaks in the lower part of each map might be attributed to $In_{0,92}Ga_{0,08}As$ or strained material with even higher In contend indicating strong relaxation in the system.

We may conclude that the fourfold symmetry of the strain field is responsible for the generation of the slight fourfold symmetric correlation of the dots which became visible in the GISAXS measurements [Fig. 1(d)]. The favorite alignment directions are the elastically weak [010] and [100] directions. The small observed compression of the correlation pattern away from the [100]/[010] correlation directions is possibly caused by residual effects from surface dynamics.

In summary, we report on fourfold symmetric 2D lateral ordering of QDs after postgrowth annealing while no ordering can be seen for the nonannealed QDs. Concluding, ordering phenomena as already been observed for growth close to thermodynamic equilibrium can also be achieved by growth away from thermodynamic equilibrium and subsequent postgrowth annealing. Elongated shape of dots, as shown recently,[8] may cause the 1D (twofold symmetric) correlation type while dots with higher symmetric bases allow to form 2D (fourfold symmetric) ordering. Postgrowth annealing may transform the dot shape from elongated to round and therefore may represent a possibility to favor either the 1D or the 2D correlation type.

The authors thank A. Singh, J. Novak, A. Diaz, and G. Buth for preparing the experimental setups at the ESRF beamlines ID10B and ID01 and the SCD beamline at ANKA. Part of the work was supported by the DFG-Center for functional nanostructures under Project No. A2.6 and DFG under Project No. SCHA 1576/1-1.

[1]M. Francardi, L. Balet, A. Gerardino, N. Chauvin, D. Bitauld, L. H. Li, B. Alloing, and A. Fiore, Appl. Phys. Lett. **93**, 143102 (2008).
[2]A. Nozik, Physica E (Amsterdam) **14**, 115 (2002).
[3]V. I. Klimov, Appl. Phys. Lett. **89**, 123118 (2006).
[4]T. W. Schlereth, C. Schneider, S. Höfling, and A. Forchel, Nanotechnology **19**, 045601 (2008).
[5]W. V. Schoenfeld, T. Lundstrom, P. M. Petroff, and D. Gershoni, Appl. Phys. Lett. **74**, 2194 (1999).
[6]X.-D. Wang, N. Liu, C. K. Shiha, S. Govindaraju, and A. L. Holmes, Jr., Appl. Phys. Lett. **85**, 1356 (2004).
[7]Z. M. Wang, H. Churchill, C. E. George, and G. J. Salamo, J. Appl. Phys. **96**, 6908 (2004).
[8]M. Schmidbauer, Z. M. Wang, Y. I. Mazur, P. M. Lytvyn, G. J. Salamo, D. Grigoriev, P. Schäfer, R. Köhler, and M. Hanke, Appl. Phys. Lett. **91**, 093110 (2007).
[9]Z. M. Wang, C. Rodriguez, S. Seydmohamadi, Y. I. Mazur, Y. Z. Xie, and G. J. Salamo, Appl. Phys. Lett. **94**, 083107 (2009).
[10]M. Hanke, M. Schmidbauer, Z. M. Wang, Y. I. Mazur, Sh. Seydmohamadi, G. J. Salamo, T. D. Mishima, and M. B. Johnson, Appl. Phys. Lett. **94**, 203105 (2009).
[11]M. Schmidbauer, S. Seydmohamadi, D. Grigoriev, Z. M. Wang, Y. I. Mazur, P. Schäfer, M. Hanke, R. Köhler, and G. J. Salamo, Phys. Rev. Lett. **96**, 066108 (2006).
[12]V. Holý, G. Springholz, M. Pinczolits, and G. Bauer, Phys. Rev. Lett. **83**, 356 (1999).
[13]G. Springholz, V. Holý, M. Pinczolits, and G. Bauer, Science **282**, 734 (1998).
[14]D. Hu, D. Schaadt, and K. Ploog, J. Cryst. Growth **293**, 546 (2006).
[15]E. Placidi, A. D. Pia, and F. Arciprete, Appl. Phys. Lett. **94**, 021901 (2009).
[16]J. Stangl, T. Roch, V. Holý, M. Pinczolits, G. Springholz, G. Bauer, I. Kegel, T. H. Metzger, J. Zhu, K. Brunner, G. Abstreiter, and D. Smilgies, J. Vac. Sci. Technol. B **18**, 2187 (2000).
[17]M. Rosini, M. C. Righi, P. Kratzer, and R. Magri1, Phys. Rev. B. **79**, 075302 (2009).
[18]X. Q. Shen and T. Nishinaga, J. Cryst. Growth **146**, 374 (1995).
[19]E. Penev, P. Kratzer, and M. Scheffler, Phys. Rev. B **64**, 085401 (2001).
[20]A. A. Matyshev and E. Fohtung, "On the computation and applications of Bessel function," arXiv:0910.0365v1 (unpublished).